Mass transfer and hydrodynamic characteristics of new carbon carbon packing: Application to CO2 post-combustion capture

Pascal Alix, Ludovic Raynal, François Abbé, Michel Meyer, Michel Prevost, David Rouzineau

Mass transfer and hydrodynamic characteristics of new carbon carbon packing: Application to CO_2 post-combustion capture

Pascal Alix[a], *Ludovic Raynal*[a], *François Abbe*[b], *Michel Meyer*[c], *Michel Prevost*[c], *David Rouzineau*[c,*]

[a] *IFP, BP.3, 69360 Solaize, France*
[b] *Snecma Propulsion Solide, Groupe Safran, Les cinq chemins 33187 Le Haillan, France*
[c] *Université de Toulouse, INPT, ENSIACET, Laboratoire de Génie Chimique (UMR 5503), 4 allée Emile Monso, BP 84234, 31432 Toulouse, France*

ABSTRACT

A novel structured packing, the 4D packing, has been characterized in terms of hydrodynamics, effective area and gas side mass transfer coefficient. The increase of the 4D opening fraction allows to reduce pressure drop and to get a better capacity than Mellapak 500Y and 750Y, for which the geometric areas are similar. The 50% open 4D packing, 4D-50%, leads to effective areas which are higher than Mellapak 500Y ones, and doubled compared with MellapakPlus 252Y ones. Effective areas for the 4D do not decrease when the opening fraction increases from 30 to 50%, this indicates that a non-negligible amount of droplets is generated at 50%. Gas side mass transfer coefficient had been measured with an original experimental method: water evaporation. Corresponding results seem to be in agreement with the literature, and with the fact that a large amount of droplets is generated. Correlations are proposed for both effective area and gas side mass transfer coefficient for the 4D-50%.

The 4D-50% packing could be very interesting for post-combustion CO_2 capture since it generates low pressure drop and a very high interfacial area. This will be further confirmed by an economic study for which the absorber plant will be designed with a rate based model.

Keywords: New packing; Post-combustion capture; Absorption; Pressure drop; Mass transfer efficiency

1. Introduction

The capture and geological storage of the CO_2 emitted by power plants is one important way to reduce greenhouse gases emissions. Huge gas flowrates must be treated for post-combustion capture of CO_2, which lead to very large capture amine plants. The optimization of such high volume reactor design is thus of great importance in order to reduce invest costs. Since capture process operates downstream the power plant, it requires very low pressure drop in order to reduce the booster fan electric consumption, operating costs and efficiency lost.

To minimize volume reactor and pressure drop, very efficient gas liquid contactors are needed. In the framework of GASCOGNE project, supported by ANR, a novel structured packing has been considered for chemical engineering studies, the "4D packing". The latter had been initially developed and is manufactured by SPS. To build-up models, tests are highly needed to characterize 4D packings in terms of hydrodynamics and mass transfer. The aim of the present study is to determine the pressure drop, the effective area, a_e, and the gas side mass transfer coefficient, k_G, for three geometric configurations. Since one assumes that MEA 30 wt% is the base case for the process (Knudsen et al., 2006; Feron et al., 2007), one can consider that fast reactions will occur in capture plants. a_e and k_G become the main parameters to estimate the efficiency of an absorber (Danckwerts, 1970). It has to be noticed that experiments have been conducted with both IFP and LGC facilities.

* *Corresponding author.*
E-mail address: david.rouzineau@ensiacet.fr (D. Rouzineau).

Nomenclature

AB	distance between two crossings of fibres
A_c	column cross-section (m^2)
a_e	effective or effective area of the packing (m^{-1})
$a_{e,4D}$	effective or effective area of the 4D packings (m^{-1})
$a_{e,void}$	effective or effective area of the IFP empty column (m^{-1})
$a_{e,global}$	effective or effective area of column section (m^{-1})
a_g	geometric area (m^{-1})
$C^0_{CO_2}$	CO_2 molar concentration in the liquid bulk ($mol\,m^{-3}$)
C_g	concentration of gas phase needed for $k_g a_e$ measurement ($mol\,l^{-1}$)
C_l	concentration of liquid phase needed for $k_g a_e$ measurement ($mol\,l^{-1}$)
C^0_{OH}	OH^- ions molar concentration in the liquid bulk ($mol\,m^{-3}$)
C^0_{Na}	Na^+ ions molar concentration in the liquid bulk ($mol\,m^{-3}$)
d	column inner diameter (m)
D_{CO_2}	CO_2 diffusion coefficient in the liquid phase ($m^2\,s^{-1}$)
D_m	diameter of the mandrel
dp	drip point density of the liquid distributor (m^{-2})
dz	height of an element of the column (m)
E	enhancement factor
$F^G_{CO_2}$	CO_2 gas molar rate ($mol\,s^{-1}$)
$F^L_{CO_2}$	CO_2 liquid molar rate ($mol\,s^{-1}$)
F_S	gas F-factor $= \sqrt{\rho_G} \times V_{sG}$ ($Pa^{0.5}$)
$F_S\|_{fl}$	gas F-factor at the flooding point ($Pa^{0.5}$)
G	gas flow rate ($kg\,h^{-1}\,m^{-2}$)
G_0	air flow ($m\,s^{-1}$)
h, h_{g,CO_2}, etc.	contributions of a cation, an anion, and a gas, respectively ($l\,mol^{-1}$)
H	column's height (m)
He	Henry constant ($Pa\,m^3\,mol^{-1}$)
H_w	Henry constant for water ($Pa\,m^3\,mol^{-1}$)
I	ionic strength of solution ($mol\,l^{-1}$)
k_2	kinetic constant ($m^3\,mol^{-1}\,s^{-1}$)
k_2^∞	infinitely diluted solution kinetic constant ($m^3\,mol^{-1}\,s^{-1}$)
k_g	gas side mass transfer coefficient ($m\,s^{-1}$)
K_G	overall gas side mass transfer coefficient ($mol\,Pa^{-1}\,m^{-2}\,s^{-1}$)
k_L	liquid side mass transfer coefficient ($m\,s^{-1}$)
L_f	width of carbon fabric
N_f	number of spindle
P	pressure, needed for $k_g a_e$ measurement (Pa)
P_{CO_2}	CO_2 partial pressure (Pa)
P_{tot}	total pressure of the column (Pa)
Q_L	liquid load ($m^3\,m^{-2}\,s^{-1}$)
S	channel side of the structured packing (m)
T	temperature (K)
T_{AS}	temperature at adiabatic conditions of saturation (°C)
T_{Gin}, T_{Gout}	inlet and outlet gas temperatures (°C)
T_{Lin}, T_{Lout}	inlet and outlet liquid temperatures (°C)
T_{ws}	water storage temperature
V_{sG}	superficial gas velocity ($m\,s^{-1}$)
Y	absolute humidity, needed for $k_g a_e$ measurement
Y_{AS}	absolute humidity at adiabatic temperature of saturation
Y_{in},Y_{out}	absolute inlet and outlet humidities of air in column
y_x	molar fraction of the component x in the gas phase (mol/mol)
z	axis column position (m)
$\Delta P/L$	pressure drop per unit length of the packed bed (Pa/m)
ΔP_{tot}	total pressure drop of the column (Pa)

Non-dimensional terms

Ha	Hatta number

Greek

θ	braid angle (°)
ε	void fraction of the bed
ϕ_{CO_2}	specific absorbed molar flux of CO_2 ($mol\,m^{-3}\,s^{-1}$)
φ_{CO_2}	absorbed molar flux of CO_2 ($mol\,m^{-2}\,s^{-1}$)
ρ_G	gas density ($kg\,m^{-3}$)

In the following, the experimental set-ups and methods are first described. Second, results are shown and discussed. Last, correlations to predict pressure drop, effective area and gas side mass transfer coefficient are proposed.

2. Methods and materials

2.1. *Packing structure*

The subject of this study focuses on a new structured packing technique (SPS Patent 2005) developed by Snecma Propulsion Solide (the SAFRAN group). It is constructed with interwoven carbon fibres (Fig. 1). The tubes are formed with carbon fabrics which are woven on a mandrel according to a particular braid angle (Fig. 2a). The braid angle (θ) corresponds to the angle formed between a braid thread and the braid axis (Fig. 2b).

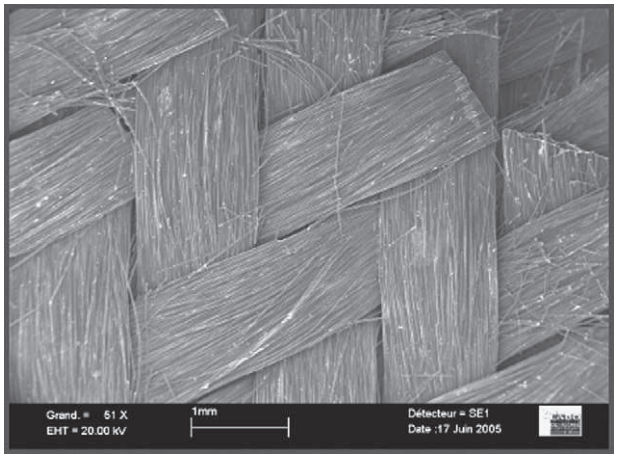

Fig. 1 – Carbon fibres woven.

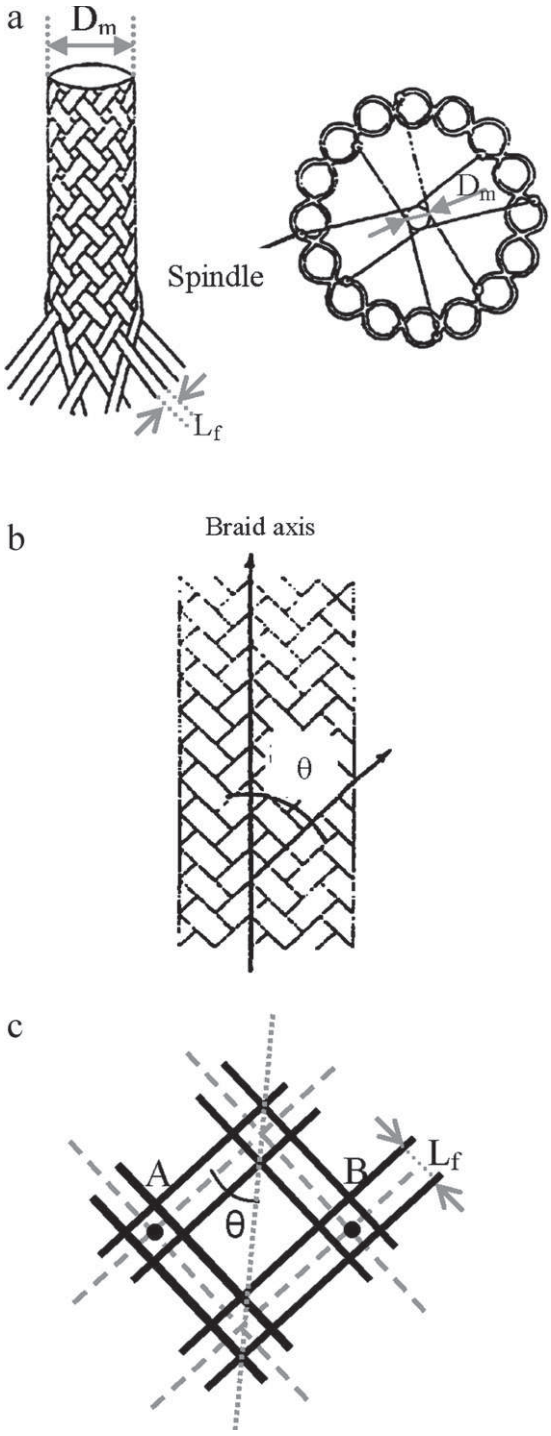

Fig. 2 – (a) Carbon fabrics woven on a mandrel; (b) braid angle; (c) crossing of fibres.

The distance between two fibre crossings (Fig. 2c) along the circumference is given by

$$AB = \frac{2\pi D_m}{N_f}, \tag{1}$$

where D_m is the diameter of the mandrel (equivalent to the diameter of a tube) and N_f is the number of spindles (Fig. 2a, 16 spindles). If

$$AB \leq \frac{L_f}{\cos\theta}, \tag{2}$$

Fig. 3 – One tube with holes.

where L_f is the width of a carbon fabric, then there is no free space between the fibres (there is no hole); but if

$$AB > \frac{L_f}{\cos\theta}, \tag{3}$$

then a hole is formed. Fig. 3 represents a tube with holes. Therefore, the value of the braid angle determines the tube hole sizes, and the lower the braid angle the bigger the holes.

The diameter of the mandrel can vary from 4.5 mm to 20 mm, and the braid angle can vary from 15° to 45°. The openings therefore swing from 0% to 85%, corresponding to a hole surface area from 0 mm^2 to 735 mm^2. The tubes are then fitted together according to the four diagonals of a cube as shown in Fig. 4a, which demonstrates why this packing is called "4D packing". Finally, the layout is repeated in the three spatial directions (Fig. 4b) to obtain the final structure (Fig. 4c).

Two packings structures were made with 10 mm diameter tubes. The first generation was made with a braid angle of 30°, so a hole size of 7.4 mm^2 (corresponding to an approximate opening of 30%; named 4D 30%, Fig. 5). This packing possesses a void fraction of approximately 94% and a geometric area, a_g, of 420 $m^2\,m^{-3}$ (the surface area is evaluated by geometrical calculation, knowing the surface of tubes, the diameter of hole and the number of tube per packing's volume in m^3). The second generation is relatively similar to the first one with only 8 spindles (N_f) instead of 12, so the hole size changes and becomes 26.6 mm^2 (relative to an approximate opening of 50%, named 4D-50%). This packing maintains a geometric area, a_g, of 330 $m^2\,m^{-3}$. Table 1 resumes the characteristics of these two packing.

This structure is advantageous because many parameters can be modified at will to optimize the performances of the structured packing. In particular, it is possible to change the tube diameters, the hole sizes of tubes (openings), the sizes of carbon fabric (number of fibres), and the tube angles. Moreover, this packing possesses other interesting properties such as a small tube thickness (0.2 mm), as suggested during the evolution of structured packing, and a significant structural cohesion (mechanical strength) due to geometry of the structure (using the four diagonals of a cube).

2.2. *IFP facilities*

Experiments have been carried out in a 0.73 m height, 150 mm internal diameter column. The pressure is close to the atmo-

Table 1 – Characteristics of the two generation of packing.						
Packing	Void fraction (tube)	D_m	N_f	L_f	a_g	Void fraction
Sepcarb® 4D-30%	31.24%	10 mm	12	2 mm	420 $m^2\,m^{-3}$	94%
Sepcarb® 4D-50%	49.84%	10 mm	8	2 mm	327 $m^2\,m^{-3}$	95%

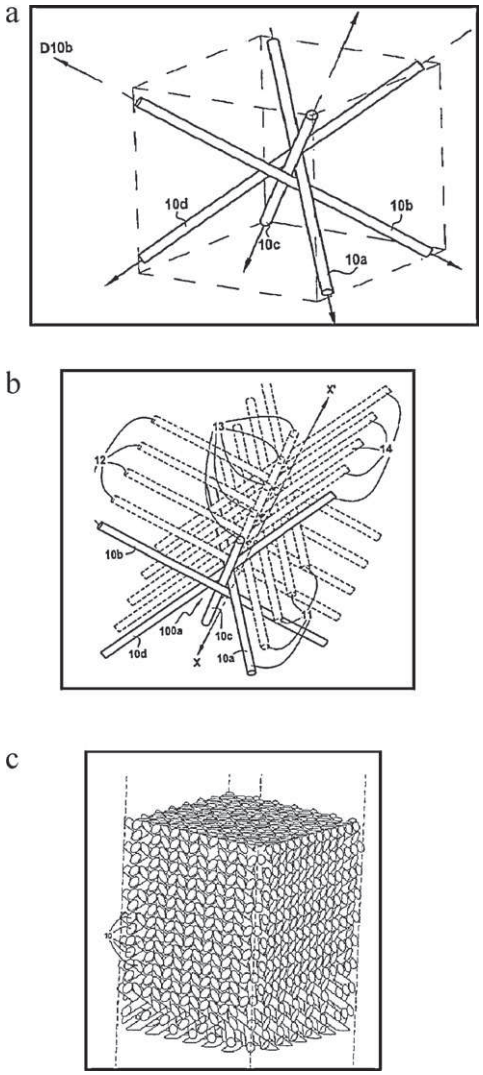

Fig. 4 – (a) Tubes fitting according to the four diagonals of a cube; (b) reproduction of the layout in one direction; (c) final structure.

Fig. 5 – 4D packing elements.

spheric pressure, the temperature is the room temperature. Liquid load, Q_L, varies from 10 to 60 $m^3\,m^{-2}\,h^{-1}$, gas velocity varies from 0 to 2 m/s which leads to a F-factor, F_s, between 0 and 2 $Pa^{0.5}$. The drip point density of the liquid distributor, *dp*, which is the number of liquid injectors by surface area, is close to 3350 m^{-2}. According to Fair and Bravo (1990) or Aroonwilas et al. (2001), it is high enough to ensure that the distributor does not influence the results.

Table 2 gives packed bed characteristics for the three tested geometries. It has to be noticed that there is a non-negligible void zone for all experiments. For the 4D-50%, a 100 mm height bloc had been tested. Elements of 4D packing are oriented at 45° from each other, and the bed heights are comprised between 0.2 and 0.6 m approximately.

2.3. *LGC facilities*

The experimental hydrodynamics and mass transfer coefficient setup for this study is a glass column with an internal diameter of 150 mm and height of 1 m. Counter current operation with an air–water system was used and all studies were carried out at room temperature and under standard atmospheric pressure. For the pressure drop measurement, the packed bed height is 0.9 m, and for the mass transfer measurement three configurations are used with bed heights comprised between 0.1 and 0.3 m approximately (see Section 2.6).

The liquid flows from a tank through a pump and flowmeter (with a measurement precision of ±2.5%) and was supplied at the top of the column via the same plate distributor provided by IFP. The liquid is again collected into the tank after having passed through the packing, with superficial liquid velocities in the range from 1 to 30 $m^3\,m^{-2}\,h^{-1}$. The gas flow is supplied at the bottom of the column and was measured by two different flowmeters (with a precision ±1.6%) for superficial gas velocities from 0 to 2 $m\,s^{-1}$ for an empty column. The pressure drop per meter was measured using an inclined U-tube filled with water, which yielded pressure measurements with a precision of 0.05 mbar.

2.4. *Pressure drop measurements at LGC*

The experimental procedure used to measure the pressure drop consists of a periodic increase of gas flow for a constant

Table 2 – Geometric characteristics of 4D beds.			
	4D-30%	4D-50%	
Configuration	1	1	2
Packed bed height (m)	0.441	0.20	0.315
Void zone height (m)	0.289	0.53	0.415
Number of blocs	9	4	5[a]
Geometric area ($m^2\,m^{-3}$)	420	327	
Void fraction (%)	94	95	
Material	Carbon		
State of surface	Smooth		

[a] A 100 mm bloc is used.

liquid flow until flooding is reached. The flooding point can be defined as the point where a reversal liquid flow appears. At this moment, the liquid is unable to flow downward through the packing, the pressure drop increases drastically, and an accurate pressure measurement is impossible due to the instability of the system. Before each test, a high liquid flow is supplied and passes through the bed for 30 min to fully wet the packing and avoid dry zones.

2.5. *Effective area measurements at IFP*

In the present study the air/NaOH system has been chosen. Within the packed column, hydroxides are consumed by the absorbed CO_2 according to the following reactions (Pohorecki and Moniuk, 1988):

$$CO_{2(G)} \leftrightarrow CO_{2(L)} \tag{4}$$

$$CO_{2(L)} + OH^- \leftrightarrow HCO_3^- \tag{5}$$

$$HCO_3^- + OH^- \leftrightarrow CO_3^{2-} + H_2O \tag{6}$$

Reaction (4) corresponds to gas to liquid absorption; reaction (5) is the reaction to consider for kinetics since reaction (6) has a much higher reaction rate than reaction (5). An enhancement factor, E, can be used to describe the impact of the chemical reaction on the absorption rate of CO_2 (Danckwerts, 1970):

$$\phi_{CO_2} = \varphi_{CO_2}.a_{e,global} = \left(\frac{1}{k_G} + \frac{He}{E.k_L}\right)^{-1}.a_{e,global}.\left(P_{CO_2} - He.C^0_{CO_2}\right)$$
$$\phi_{CO_2} = K_G.a_{e,global}.\left(P_{CO_2} - He.{C_{CO_2}}^0\right) \tag{7}$$

At column inlet, the CO_2 molar fraction in the gas phase is close to 400 ppmv, while the concentration of NaOH in the liquid phase is equal to 0.1 mol l^{-1} and in large excess compared to the absorbed CO_2. During a test, a 1 m^3 storage tank ensures that the sodium hydroxide and bicarbonates concentrations are constant and negligible, respectively (Raynal et al., 2004). This leads to a pseudo-first order reaction and fast reaction regime (Seibert et al., 2005; Alix and Raynal, 2008) for which (Danckwerts, 1970):

$$\begin{cases} E = Ha = \dfrac{\sqrt{D_{CO_2}.k_2.C^0_{OH}}}{k_L} \\ C^0_{CO_2} = 0\,\text{mol m}^{-3} \end{cases} \tag{8}$$

It can also be assumed that the gas side resistance is negligible. Without gas resistance, the combination of relations (7) and (8) gives:

$$\phi_{CO_2} = \frac{\sqrt{D_{CO_2}.k_2.C^0_{OH}}}{He}.P_{CO_2}.a_{e,global} \tag{9}$$

Within the packed column, one-dimensional and stationary plug flows of liquid and gas are assumed. Then, the packed bed can be simulated by a succession of single elements (Fig. 6) for which the mass balance leads to the following set of equations:

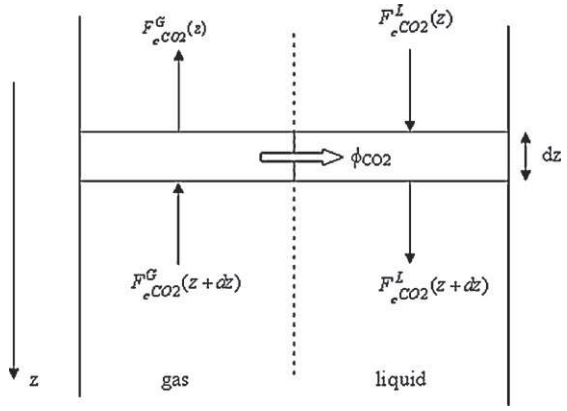

Fig. 6 – Single element to model packed bed of experimental columns, and estimate mass transfer parameters.

$$\begin{cases} \dfrac{dF^G_{CO_2}}{dz} = \phi_{CO_2}.A_c \\ F^G_{CO_2} = \dfrac{y_{CO_2}}{1 - y_{CO_2}} \times F^G_{N_2} \\ y_{CO_2} = \dfrac{P_{CO_2}}{P_{tot}} \end{cases} \tag{10}$$

The CO_2 gas molar fraction is measured at the inlet and at the outlet of the column via infrared measurements. The effective area of the column section, $a_{e,global}$, is assumed to be constant. The column is assumed to be isotherm and isobar, this is justified by the small amount of CO_2 which is absorbed, the negligible corresponding temperature increase, and the very little pressure drop. Diffusion coefficient, D_{CO_2}, kinetic constant, k_2, and Henry constant, He, have been calculated with relations given by Pohorecki and Moniuk (1988). For the present chemical system, the sodium hydroxide solution can be considered unloaded, and the liquid viscosity is close to the water viscosity. This leads to:

$$\begin{cases} \log\left(\dfrac{H_w}{He}\right) = -I \times h = -\dfrac{1}{2000}\left(C^0_{Na} + C^0_{OH}\right) \times (0.091 + 0.066 + h_{g,CO_2}) \\ \log\left(\dfrac{100}{H_w}\right) = 9.1229 - 5.9044 \times 10^{-2} \times T + 7.8857 \times 10^{-5} \times T^2 \\ \log\left(\dfrac{k_2}{k_2^\infty}\right) = 0.0221 \times I - 0.016 \times I^2 \\ \log(k_2^\infty) = 11.895 - \dfrac{2382}{T} \\ \log(D_{CO_2}) = -8.1764 + \dfrac{712.5}{T} - \dfrac{2.594 \times 10^5}{T^2} \end{cases} \tag{11}$$

From the inlet CO_2 molar fraction, $y_{CO_2,in}$, relations (9) and (10) show that $a_{e,global}$ is the only parameter to adjust in order to fit the CO_2 outlet molar fraction. Then the CO_2 profile directly gives $a_{e,global}$.

Liquid samples are taken at inlet and at outlet of the column. CO_2 content is measured by HCl titration. Mass balance between the gas and the liquid phase has thus been checked.

2.6. *Gas side mass transfer coefficient measurements at LGC*

Generally used methods of $k_g a_e$ determination can be classified into three main categories:

- the absorption of a gas/vapour soluble in liquid-phase

Table 3 – Different methods used in the literature for $k_g a_e$ determination.

	Absorption	Evaporation of pur liquid	Absorption with chemical reaction
Examples	Air-CO_2[a] or SO_2[a] or NH_3[a] or O_2[b]/water	Air/water or methanol[c] or MEK…	NH_3[d]/H_2SO_4 SO_2[a]/NaOH
Obligation	Humidification of gas		Humidification of gas
Measurements	C_g, C_l, T, P, Y[e,f,g]	T, P, Y[e,f,h]	C_l, C_g, T, P, Y[e,f,g]
Difficulties	C_g, C_l, no isotherm	$T_{interface}$[h,i,j]	C_g, C_l, no isotherm

[a] Billet (1995).
[b] Puranik and Vogelpohl (1974).
[c] Surosky and Dodge (1950).
[d] Nakov and Kolev (1994).
[e] Vidwans and Sharma (1967).
[f] Sharma and Dankwerts (1970).
[g] Hüpen et al. (2006).
[h] Treybal (1965).
[i] Onda et al. (1968).
[j] Kawasaki and Hayakawa (1972).

- the evaporation of a pure liquid by an inert gas,
- the absorption with chemical reaction.

Table 3 gives the different systems used in the literature for the determination of $k_g a_e$, and the need of measurement and the difficulties of each method are presented.Following the analysis of this table, the method of evaporation of pure liquid is applied here to water as the pure liquid and to air as the inert gas; despite the fact that the method is less used nowadays, it presents however some advantages. Indeed, using the method of evaporation of pure liquid, we ensure that the transfer resistance is totally limited to gas-phase.

However, it is recognized that depending on operating conditions and in cases of absorption with chemical reaction mass transfer resistance is practically confined to the gas phase. The process by physical absorption is not satisfying, because it does not allow to reduce sufficiently the liquid film resistance in order to obtain $k_g a_e$. However, the number of measurement carried out for the method of evaporation of a pure liquid is low compared to other two methods, which limits a priori the uncertainties evaluation of $k_g a_e$.

Regarding the quality of results one can expect from this method, the article of Surosky and Dodge (1950) can serve as a reference because it is comprehensive, full of useful information and details a clear methodology treatment of raw experimental values. The results show that it is possible to have a precision on the $k_g a_e$ of 10%. Moreover, the measurement of air humidity is nowadays achieved with more efficient equipment.

The operating mode is to obtain adiabatic conditions of saturation by taking into contact the air with water at counter-current under steady-state conditions. The air humidification as cooling procedure leads the system towards a stable operating conditions in terms of water temperature at adiabatic conditions of saturation (T_{AS}). The gathered experimental data's at stable condition of functioning permit the determination of $k_g a_e$, using mass balance for gas-phase:

$$\mathrm{Ln}\frac{Y_{AS}-Y_{in}}{Y_{AS}-Y_{out}} = k_g a_e \frac{H}{G_0} \quad (12)$$

With Y_{in} and Y_{out} as absolute inlet and outlet humidities of air in column, G_0 as air flow, Z as column's height and Y_{AS} as absolute humidity at adiabatic temperature of saturation. In order to overwhelm the impact of extremity effects, authors (Surosky and Dodge, 1950) recommend realising the same measurements with at least two different heights of packing. So, our pilot contains a column of 150 mm diameter, with water and air at counter-current (Fig. 7). Dry air flow is measured; then it is humidified and heated (by an evaporator fed by a measuring micro-pump) in order to obtain desired conditions of bottom-column.

Temperature and dew point are measured at inlet and outlet sections by a hygrometer (hygrometer with cooled mirror permitting an accuracy of $\pm 0.1\,^{\circ}C$ of the dew point). Water circulates in closed loop through storage, up-column, liquid distributor (with adjustable height to distribute 5 cm on top the packing), gas distributor to come back into storage. Flows, inlet and outlet temperatures of column (T_{Lin} and T_{Lout} for liquid temperature and T_{Gin} and T_{Gout} for gas temperature), absolute inlet and outlet humidities of air (Y_{in} and Y_{out}), as well as storage temperature (T_{ws}) are measured (Fig. 7). The liquid storage has to be so limited in terms of volume (10 l) in order to reduce the time of stabilisation. The operating conditions are predicted to obtain an adiabatic temperature of saturation close to the surrounding temperature.

For each test, the steady state is reached (observed after 30 min when all measurements are stable). In this case, the temperatures T_{Lin}, T_{Lout} and T_{ws} are equal, and adiabatic temperature of saturation is reached. This temperature permits to calculate Y_{AS}, the absolute humidity at adiabatic temperature of saturation. And the final result $k_g a_e$ is calculated by the relation (12).

For the present study six 4D-30% and 4D-50% blocs had been tested.

3. Results and discussion

3.1. *Pressure drop curve*

Fig. 8 gives the dry pressure drop of 4D packings as a function of the F-factor. Logarithmic scales are used in order to check the pressure drop power law coefficient which is linked to the flow regime. Present measurements are compared with calculated pressure drop for three Mellapak structured packings commercialized by Sulzer Chemtech: M252Y, M500Y and M750Y. It has to be noticed that the geometric areas of selected commercial packings are closed to the 4D ones (see Tables 2 and 4). Calculations have been carried out with the manufacturer software Sulcol 2.0. First, the experimental pres-

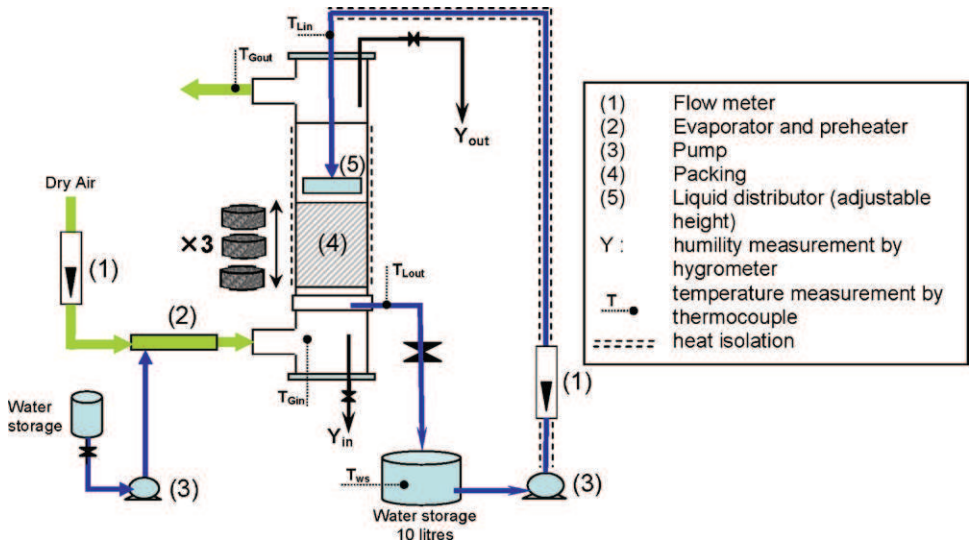

Fig. 7 – Experimental setup for $k_g a_e$ measurement.

Table 4 – Geometric characteristics of tested Mellapak packings for effective area measurement.

	MellapakPlus 252Y	Mellapak 250Y[a]	Mellapak 500Y[a]
Packed bed height (m)	2	3	3
Column diameter (m)	0.15	0.43	0.43
Geometric area ($m^2\ m^{-3}$)	250	250	500
Void fraction (%)	98	98	97.5
Corrugation length (mm)	19	19	9
Channel angle (°)	45	45	45
Material	316L		
State of surface	Texture on the wall, perforated		

[a] Tsai et al. (2008).

sure drop on a column equipped with 4D-30% is similar to the one calculated on a column equipped with Mellapak 750.Y. Second, the use of the 4D-50% allows to reduce the pressure drop by 50% approximately. The pressure drop on a column equipped with 4D-50% becomes similar to the one calculated on a column equipped with Mellapak 500Y. It has to be noticed that the slope of the curve is close to 1.9 for both 4D-30% and 4D-50%, this result is similar to the results obtained by Spiegel and Meier (1992). Last, the calculated pressure drop on a column equipped with MellapakPlus 252.Y, which is the reference case for the present work, is 50% lower than the one measured on a column equipped with 4D-50%.

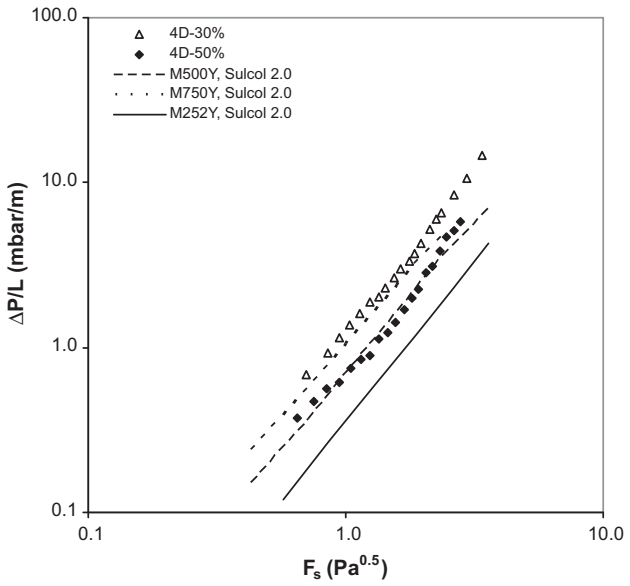

Fig. 8 – Dry pressure drop as a function of Fs for 4D open packings. Comparison with calculated pressure drop for Mellapak 750Y, Mellapak 500Y and MellapakPlus 252Y (Sulcol 2.0).

Fig. 9 gives the wetted pressure drop of 4D packings as a function of the F-factor and for $Q_L = 28\ m^3\ m^{-2}\ h^{-1}$. Such liquid load is expected for CO_2 absorbers. Present measurements are compared with calculated pressure drop for Mellapak 252Y, 500Y and 750Y. In the case of 4D packings, the pressure drop is reduced by 30% while the capacity is increased by 25% when the opening fraction increases from 30 to 50%. Below the loading point, the experimental pressure drop on a column equipped with 4D-30% (respectively 4D-50%) is similar to the one calculated on a column equipped with Mellapak 750.Y (respectively 500Y). The flooding limit of the 4D-30% is similar to the one given for Mellapak 750Y, and the flooding limit of the 4D-50% is higher than those given for Mellapak 500Y and 750Y. For a column equipped with 4D-50% which operates at a flooding percentage equals 70%, the packed bed pressure drop will be close to 3 mbar/m. Last, it should be noticed that the capacity of the MellapakPlus 252Y is 40% higher than the 4D-50% one.

3.2. *Effective area*

First, the void zone impact should be characterized for open 4D packing (cf. Table 2). Fig. 10 gives effective area which has

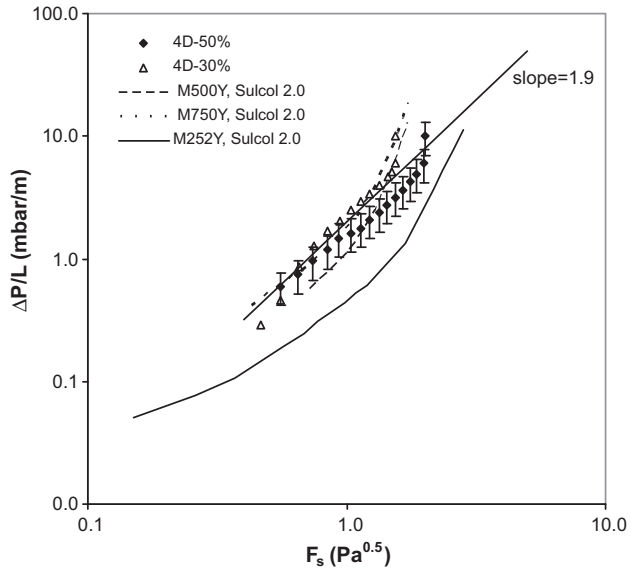

Fig. 9 – Wetted pressure drop as a function of *Fs* for 4D open packings, *QL* = 28 m³ m⁻² h⁻¹. Comparison with calculated pressure drop for Mellapak 750Y, Mellapak 500Y and MellapakPlus 252Y (Sulcol 2.0).

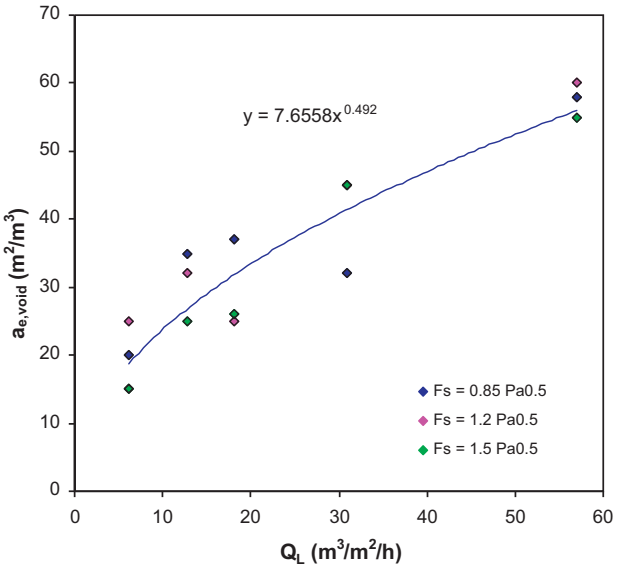

Fig. 10 – Effective area for the void zone, as a function of *QL* and *Fs*.

been measured with an empty column, $a_{e,void}$, as a function of Q_L and F_s. First, it appears that $a_{e,void}$ does not depend on the gas flowrate for the tested range. Second, $a_{e,void}$ is low and comprised between 20 and 60 $m^2\ m^{-3}$. Last, a simple and accurate correlation can be used to estimate $a_{e,void}$ for the present work:

$$a_{e,void} = 7.66 \times (3600 \times Q_L)^{0.492} \quad (13)$$

CO_2 absorbed rate measurements give the averaged effective area for the entire column, $a_{e,global}$ (see Section 2.5).

For the 4D-30% and 4D-50% packings, the void zone cannot be neglected (see Table 2) and the packed bed effective area will be given by:

$$a_{e,4D} = \frac{a_{e,global} \times H - a_{e,void} \times (H - H_{4D})}{H_{4D}} \quad (14)$$

Two configurations have been tested with the 4D-50% (see Table 2), then relation (14) leads to two different values for $a_{e,4D}$. For this work, an arithmetic average of these two values is retained. Fig. 11 gives the effective area measured with the 4D packings as a function of F_s and Q_L. Present experiments are compared with effective areas measured for different commercial packings: MellapakPlus 252.Y (Alix and Raynal, 2009), Mellapak 250Y and 500Y (Tsai et al., 2008). It has to be noticed that MellapakPlus 252.Y had been characterized with the same experimental column as 4D packings, however 2% CO_2/1N sodium hydroxide system was used. The latter could lead to underestimate the effective area about 15% because of gas lim-

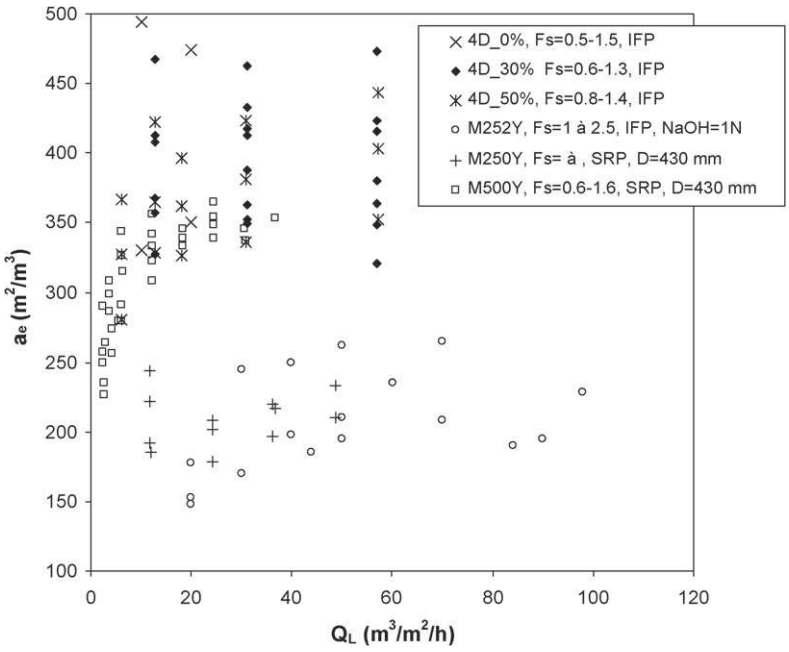

Fig. 11 – Effective area for 4D packings as a function of *QL*. Comparison *with* different Mellapak commercial packings (Alix and Raynal, 2009; Tsai et al., 2008).

itation and non-pseudo-first order reaction (Alix and Raynal, 2008). It has to be also noticed that Mellapak 250.Y and 500.Y had been characterized by SRP with a 430 mm diameter column. The use of different column diameters could impact experimental results (Olujic, 1999), however, since the column diameters are always much higher than channel sizes (see Table 4), the diameter impact should be moderate (Henriques de Brito et al., 1994). First, one can observe that MellapakPlus 252.Y and Mellapak 250.Y effective areas are similar, this was expected since both packings have very similar geometric characteristics (see Table 4). This result indicates that chemical system and diameter effects should be moderate for this packing, then it is reasonable to compare present results with those obtained with Mellapak 250.Y and MellapakPlus 252.Y. Since Mellapak 500Y channel size is lower than the Mellapak 250.Y one (see Table 4), scale effect should be lower for the 500.Y. This also indicates that it is reasonable to compare present results with those obtained with Mellapak 500.Y.

Second, Fig. 11 shows that, whatever the opening fraction, 4D effective areas are similar while a_g decreases strongly when the opening fraction increases. This result could be explained by the fact that more droplets are generated when opening fraction increases (Alix and Raynal, 2008). Then, the effective area could exceed the geometric one for 4D-50% (ratio up to 1.4). Third, experimental values are more scattered for 4D packing than those obtained with Mellapak packings. This is explained by the fact that the effective area is less sensitive to the gas flowrate for Mellapak than for 4D packings. In the case of open 4D packings, the gas flowrate impact is linked to the amount of droplets like for random packings. Last, 4D interfacial areas are much higher than those obtained with Mellapak packings in spite of the fact that the Mellapak geometric areas could exceed 4D ones. This result is very interesting since the absorber height will be directly linked to the packing effective area, and this efficiency gain could compensate the lower capacity of 4D packings (see Section 3.1). The 4D-50% structure is the more interesting geometry since it gives the best compromise between efficiency and capacity.

To estimate the gain relatives to 4D-50% packing for CO_2 capture plants, one should model the overall absorber (including hydrodynamics, mass and heat transfer, thermodynamics, and kinetic). Then, a correlation to estimate the interfacial area is highly needed. Fig. 12 gives the effective area for the 4D-50% packing as a function of F_s and Q_L. The following relation can be given with an accuracy of ±5%:

$$\begin{cases} a_{e,4D\text{-}50\%} = A \times (3600 \times Q_L)^B \\ A = 137.77 \times F_s + 134.39 \\ B = 0.085 \end{cases} \quad (15)$$

3.3. *Gas side mass transfer coefficient*

$k_g a_e$ measurements are realised with 3 different heights of packing in order to deduce the extremity effects, i.e. 1 blocs, 2 blocs and 3 blocs of packing (0.1 m, 0.2 m, and 0.3 m, respectively). First, the packing 4D-50% had been tested for a liquid load scale of 7–23 $m^3\,m^{-2}\,h^{-1}$, and for a gas flow rate scale of 3500–7200 $kg\,m^{-2}\,h^{-1}$.

The values of $k_g a_e$ are presented in logarithmic scale as a function gas flow rate's logarithm in Fig. 13. Regarding this figure, two straight lines (dotted) are added which correspond at +10% and −10% of the average value, and points are included between these two boundaries.

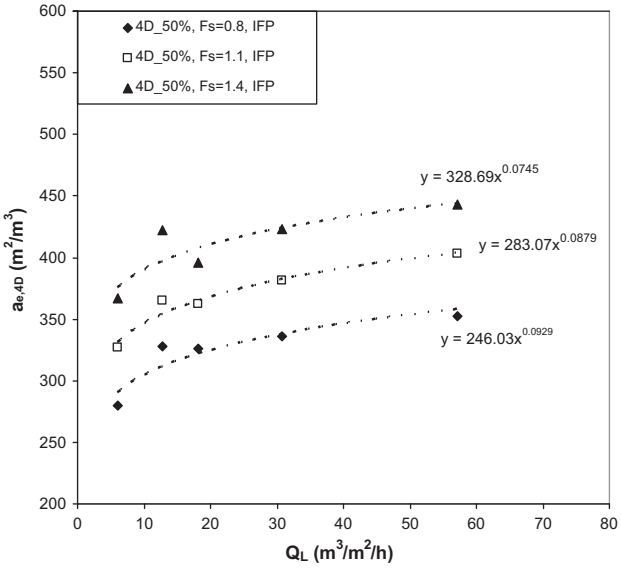

Fig. 12 – Effective area for 4D-50% as a function of *Fs* and *QL*.

Therefore, under functional conditions of this packing, the results present a quasi-independency on liquid flow rate, and an important dependency on gas flow rate. The following relationship is then suggested:

$$k_g * a_e = 3.7488 \times 10^{-3} * G^{0.843} \quad (16)$$

with G in $kg\,h^{-1}\,m^{-2}$ and $k_g{}^* a_e$ in s^{-1}.

The power of G is around 0.8 against 0.7 for most of traditional packing (Onda et al., 1968). Even if it is not traditional, it has been already observed for some other internals of column. According to Dwyer and Dodge (1941), the dependency on gas flow rate for rings with 25 mm diameter is a power of 0.77 and for 12.5 mm ring diameter is 0.9. For the 4D packing, the tube diameter is 10 mm which is closed to the 12.5 mm ring diameter. That is suggesting that for the 4D-50% the characteristic dimension of flow is low and the tests in 150 mm column diameter are representative.

However, it is possible that this value is linked to the fact that a_e is very sensitive to the gas flowrate. Regarding its particular structure, this packing generates:

- liquid droplets through large openings.
- liquid film which follows the assembly angle of packing tubes and therefore an increase in movement with respect to a vertical flow.

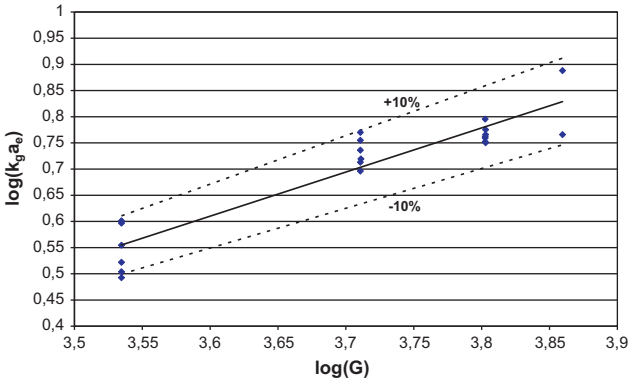

Fig. 13 – Dependency of log($k_g a_e$) as a function of log(*G*) for 4D-50%.

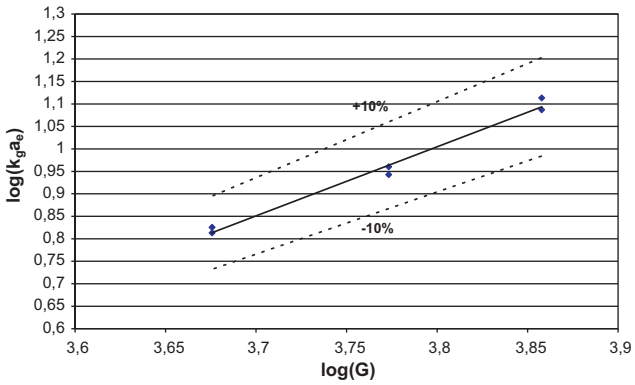

Fig. 14 – Dependency of log($k_g a_e$) on log(G) for the 4D-30%.

- the possibility of creating the equivalent of a bubbling in the middle of tubes of packing structure at high gas flow rates, with maybe a possible liquid upstream in the channels formed by tubes.

Second, the 4D-30% packing is tested with a liquid load equals 16 $m^3\,m^{-2}\,h^{-1}$ and the previous range of gas flow rate. The results are illustrated in logarithmic scale in Fig. 14. One can observe a high dependency on LOG(G) (1.54 power of G), as for the 4D-50%. This could be also explained by the fact that a_e is very sensitive to the gas flowrate.

$$k_g * a_e = 1.4612 \times 10^{-5} * G^{1.54} \quad (17)$$

with G in $kg\,h^{-1}\,m^{-2}$ and $k_g{}^* a_e$ in s^{-1}.

4. Conclusions and perspectives

A novel structured packing, the 4D packing, had been characterized in terms of hydrodynamics and mass transfer. The 4D packing is made of carbon tubes which could be opened by adjusting manufacturing parameters (such as braid angle). With an opening fraction of 50%, the capacity of the 4D packing is maximum and becomes better than those given for Mellapak 500Y and 750Y which have similar geometric areas. However the capacity of the 4D-50% is 40% lower than the one given for the MellapakPlus 252.Y which is our reference case.

The effective area of the 4D packing, a_e, does not decrease when the opening fraction increases from 30 to 50%. This indicates that more droplets are generated with the 4D-50%, this is confirmed by the fact that a_e becomes more sensitive to the gas flowrate 4D-50%. The effective area is much higher than those measured with Mellapak packings. In particular, the effective area is doubled compared to the MellapakPlus 252Y one. Then the 4D-50% packing should be very efficient for CO_2 capture. This should at least compensate the lower capacity of the 4D-50%.

The gas side mass transfer coefficient, k_G, had been measured for 4D packing via water evaporation. This original method gives very accurate results. Correlations are given to estimate a_e and $k_G{}^* a_e$. These correlations will be used afterwards to provide a rate-based model for the absorber (Aspen ratesep). The model shows the performance of 4D packing in CO_2 capture with 30 wt% MEA. Experiments will be also conducted with a 400 mm diameter column in order to valid present results in terms of pressure drop curves and effective area.

Acknowledgments

This work is supported by ANR (French National Research Agency) through the GASCOGNE project.

The authors would like to thank the ANR for its financial support under the GASCOGNE project.

References

Alix, P., Raynal, L., 2008. Pressure drop and mass transfer of a high capacity random packing. Application to CO_2 post-combustion capture. In: GHGT-9 Congress, Washington, DC.

Alix, P., Raynal, L., 2009. Characterization of a high capacity structured packing for CO_2 capture. In: WCCE8 Congress, Montreal.

Aroonwilas, A., Tontiwachwuthikul, P., Chakma, A., 2001. Effects of operating and design parameters on CO_2 absorption in columns with structured packings. Separation and Purification Technology 24, 403–411.

Billet, R., 1995. Packed Towers, Weinheim.

Danckwerts, P.V., 1970. Gas Liquid Reaction. McGraw-Hill, New York.

Dwyer, O.E., Dodge, B.F., 1941. Rate of absorption of ammonia by water in a packed tower. Industrial and Engineering Chemistry 33, 485.

Fair, J.R., Bravo, J.L., 1990. Distillation columns containing structured packing. Chemical Engineering Progress 86 (1), 19–29.

Feron, P.H.M., Abu-Zahra, M., Alix, P., Biede, O., Broutin, P., de Jong, H., Kittel, J., Knudsen, J., Raynal, L., Vilhelmsen, P.J., 2007. Development of post-combustion capture of CO_2 within the CASTOR Integrated Project: results from the pilot plant operation using MEA. In: 3th International Conference on Clean Coal Technologies for our Futur, Cagliari, Italy.

Henriques de Brito, M., von Stockar, U., Menendez Bangerter, A., Bomio, P., Laso, M., 1994. Effective mass-transfer area in a pilot plant column equipped with structured packings and with ceramic rings. Industrial and Engineering Chemistry Research 33, 647–656.

Hüpen, B., Hoffmann, A., Gorak, A., Löning, J.-M., Haas, M., Runowski, T., Hallenberger, K., 2006. Institution of Chemical Engineers, Symposium Series No. 152, 523.

Kawasaki, J., Hayakawa, T., 1972. Direct contact mass and heat transfer between vapor and liquid with change of phase. Journal of Chemical Engineering of Japan 5 (2), 119.

Knudsen, J.N., Vilhelmsen, P.J., Jensen, J.N., Biede, O., 2006. First year operation with 1t/h CO_2 absorption pilot plant at Esbjerg coal-fired power plant. In: VGB Conference, Chemie im Kraftwerk, 11–12 October, Bad Neuenahr, Germany.

Nakov, S., Kolev, N., 1994. Performance characteristics of a packing with boundary layer turbulizers. IV. Gas film controlled mass transfer. Chemical Engineering and Processing 33, 437.

Olujic, Z., 1999. Effect of column diameter on pressure drop of a corrugated sheet structured packing. TransICheme 77A, 505–510.

Onda, K., Takeuki, H., Okumoto, Y., 1968. Mass transfer coefficients between gas and liquid in packed columns. Journal of Chemical Engineering of Japan 1 (1), 56.

Pohorecki, R., Moniuk, W., 1988. Kinetics of reaction between carbon dioxide and hydroxyl ions in aqueous electrolyte solutions. Chemical Engineering Science 43 (7), 1677–1684.

Puranik, S.S., Vogelpohl, A., 1974. Effective interfacial area in irrigated packed columns. Chemical Engineering Science 29 (2), 501–507.

Raynal, L., Ballaguet, J.P., Barrere-Tricca, C., 2004. Determination of mass transfer characteristics of co-current two phase flow within structured packing. Chemical Engineering Science 59, 5395–5402.

Seibert, F., Wilson, I., Lewis, C., Rochelle, G., 2005. Effective gas/liquid contact area of packing for CO_2

absorption/stripping. Greenhouse Gas Control Technologies II, 1925–1928.
Sharma, M.M., Dankwerts, P.V., 1970. Chemical methods of measuring interfacial area and mass transfer coefficients in two fluids systems. British Chemical Engineering 15 (4), 522.
Spiegel, L., Meier, W., 1992. A generalized pressure drop model for structured packings. ICheme Symposium Series, no. 128, B85–B91.
SPS: patent FR 0511051 (2005).
Surosky, A.E., Dodge, B.F., 1950. Effect of diffusivity on gas-film absorption coefficients in packed towers. Industrial and Engineering Chemistry 42 (6), 1112.
Treybal, R.E., 1965. Mass Transfer Operations. McGraw-Hill Company.
Tsai, R., Schultheiss, P., Kettner, A., Lewis, C., Seibert, F., Eldridge, B., Rochelle, G., 2008. Influence of surface tension on effective packing area. Industrial and Engineering Chemistry Research 47 (4), 1253–1260.
Vidwans, A.D., Sharma, M.M., 1967. Gas-side mass transfer coefficient in packed columns. Chemical Engineering Science 22, 673.